

Supporting Information

Experimental Details

Synthetic procedure

Synthesis of $[\text{Fe}_{15}\text{O}_6(\text{tea})_8\text{Cl}_6](\text{OH})(\text{ClO}_4)_2$ (1)

FeCl_3 (0.162 g, 1 mmol) and $\text{Fe}(\text{ClO}_4)_2 \cdot 6\text{H}_2\text{O}$ (0.254 g, 1 mmol) were dissolved in methanol (25 cm^3). Triethanolamine (0.198 cm^3 , 1.5 mmol) was added dropwise to the orange solution. Triethylamine (0.418 cm^3 , 3 mmol) was added dropwise and the darkened solution was stirred at room temperature overnight. The dark orange solution was then filtered under gravity and 12.5 cm^3 samples of the filtrate were transferred to Teflon-lined autoclaves and heated to 100°C for 24 hrs. The reaction vessels were left to cool and stand for 48 hrs yielding dark red rod-shaped crystals suitable for X-ray diffraction. Yield = 0.096 g [0.041 mmol] (31.5% by Fe). Elemental analysis (% C H N) calculated (found) for $\text{C}_{48}\text{H}_{97}\text{Cl}_8\text{Fe}_{15}\text{N}_8\text{O}_{39}$: C 24.71 (24.35), H 4.18 (4.28), N 4.84 (4.40).

Single Crystal X-ray Diffraction

Diffraction data for **1** was collected using a Oxford Diffraction Xcalibur diffractometer with MoK α radiation, and is given in Table S1. An Oxford Cryosystems Cryostream 700+ low temperature device was used to maintain a crystal temperature of 120.0 K. The structure was solved using ShelXT and refined with version ShelXL interfaced through Olex2.^{1,2} All non-hydrogen atoms were refined using anisotropic displacement parameters. H atoms were placed in calculated positions geometrically and refined using the riding model. CCDC = 2090901.

Compound (1)			
Formula	$\text{C}_{48}\text{H}_{97}\text{Cl}_8\text{Fe}_{15}\text{N}_8\text{O}_{39}$	Z'	0.166667
$D_{\text{calc.}}/\text{g cm}^{-3}$	2.014	Wavelength/ \AA	0.71073
μ/mm^{-1}	2.865	Radiation type	Mo K α
Formula Weight	2531.68	$\Theta_{\min}/^\circ$	3.363
Colour	dark red	$\Theta_{\max}/^\circ$	29.352
Shape	block-shaped	Measured Refl's.	15300
Size/ mm^3	$0.80 \times 0.50 \times 0.30$	Indep't Refl's	3385
T/K	120.0(2)	Refl's. $I \geq 2 \sigma(I)$	2914
Crystal System	trigonal	R_{int}	0.0219
Space Group	$R\bar{3}$	Parameters	304
$a/\text{\AA}$	15.1578(5)	Restraints	276
$b/\text{\AA}$	15.1578(5)	Largest Peak	1.681
$c/\text{\AA}$	31.4738(12)	Deepest Hole	-1.385
$\alpha/^\circ$	90	GooF	1.134
$\beta/^\circ$	90	wR ₂ (all data)	0.1401
$\gamma/^\circ$	120	wR ₂	0.1349
$V/\text{\AA}^3$	6262.6(5)	R_1 (all data)	0.0756
Z	3	R_1	0.0646

Table S1. Single crystal X-ray diffraction data for complex **1**.

Supporting Information

Powder X-ray Diffraction

Diffraction data were collected on polycrystalline powders using a Bruker D2 PHASER with nickel filtered Cu radiation at power 30 kW and current 10mA. Diffraction measured from $2\theta = 5^\circ - 50.021^\circ$; step size, 0.0162° ; time per step, 0.525 s.

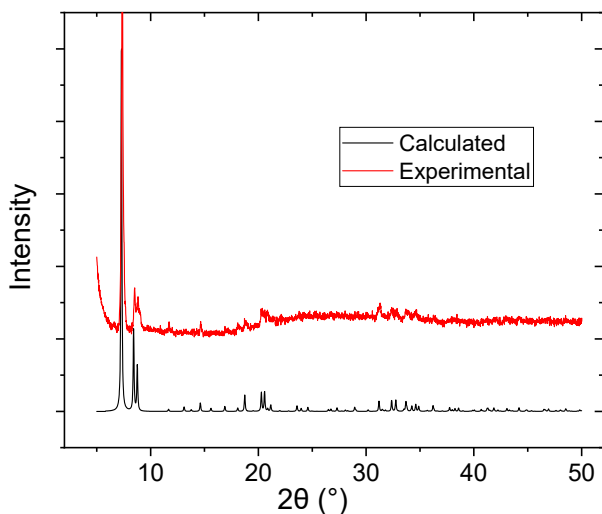


Figure S1. Powder X-ray diffraction of **1**. Experimental data (red) and calculated (black) data.

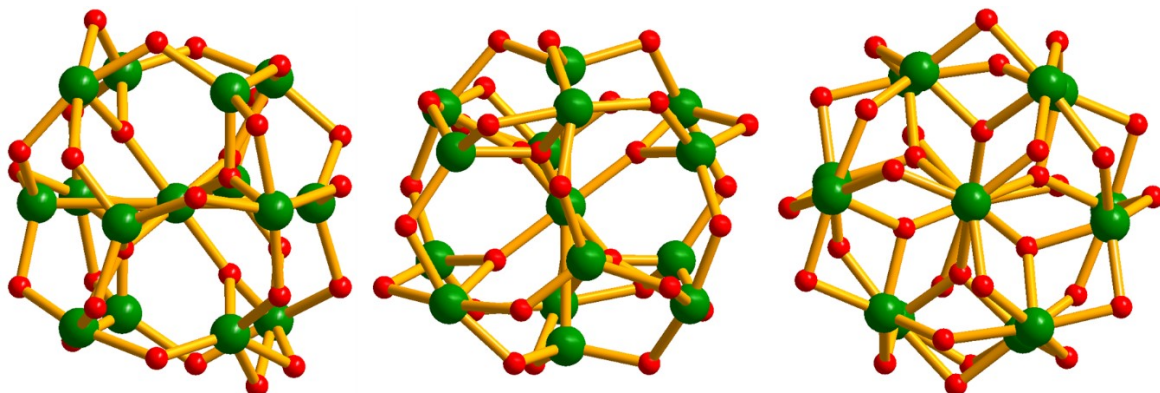


Figure S2. Orthogonal views of the metal-oxygen core of **1**, down the (left to right) *a*-, *b*- and *c*-axis of the unit cell.

Supporting Information

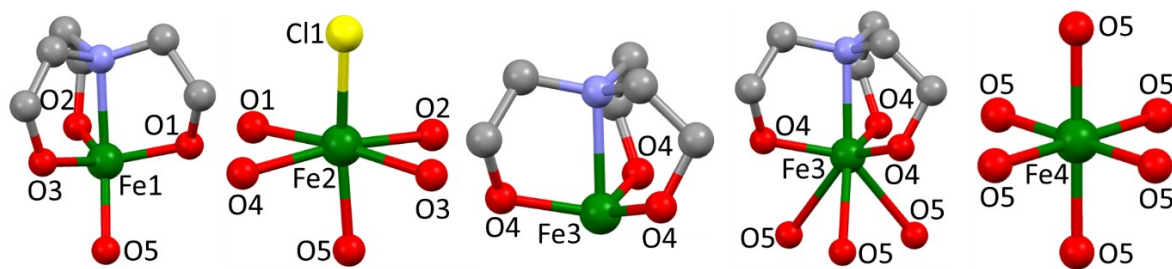


Figure S3. Metal coordination at the four symmetry inequivalent Fe ions. Fe1 = five coordinate, trigonal pyramidal; Fe2 = six coordinate, octahedral; Fe3 = four coordinate, trigonal prism or seven coordinate, capped octahedron if the Fe-O5 bonds are included; Fe4 = octahedral. Colour code: Fe = green, O = red, N = blue, C = grey, Cl = yellow. H-atoms omitted.

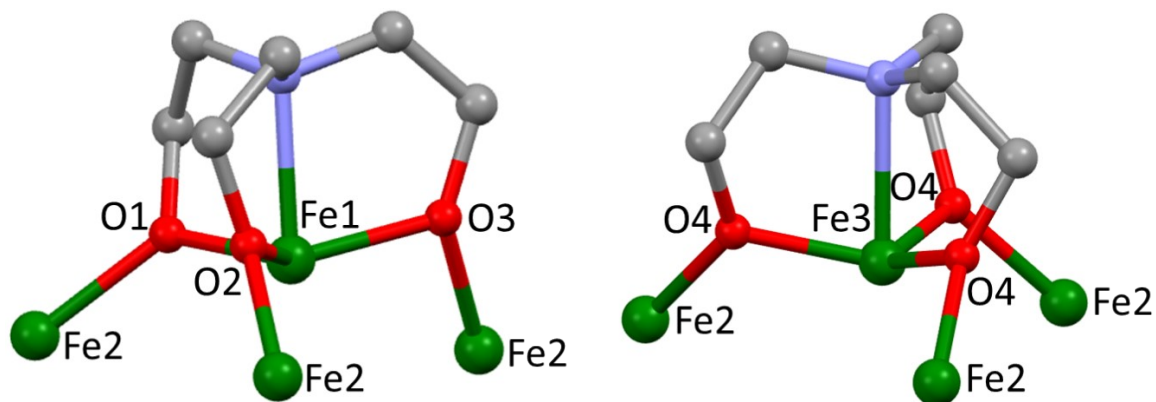


Figure S4. Coordination/bridging mode of the tea³⁻ ligands bonded to Fe1 and Fe3. Colour code: Fe = green, O = red, N = blue. H-atoms omitted.

Supporting Information

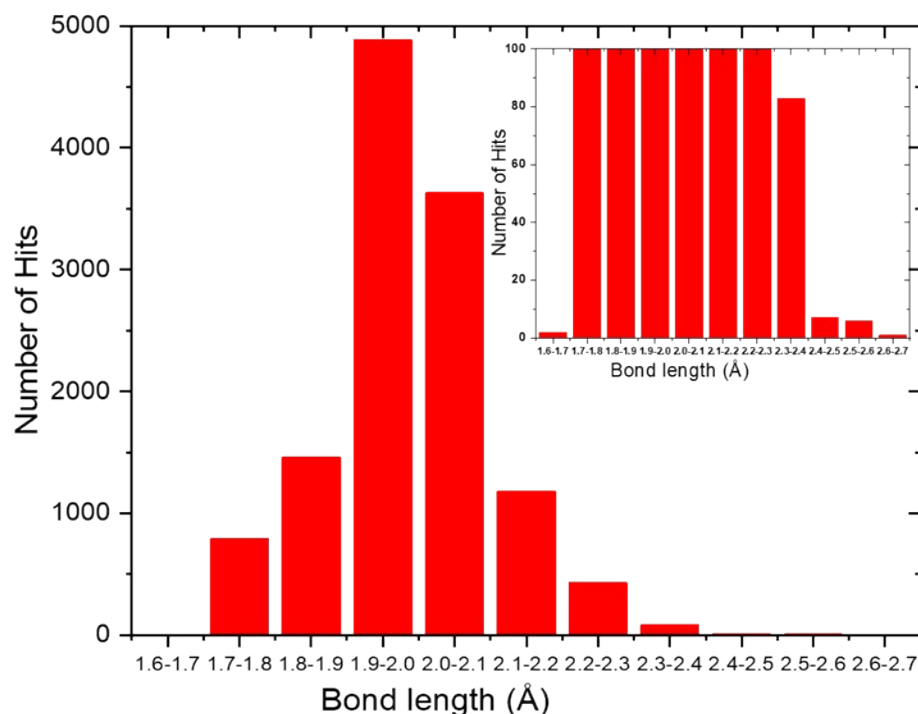


Figure S5. Histogram showing the hits resulting from a bond length search of the Cambridge Structural Database for compounds containing the Fe-O-Fe moiety, with no other restrictions. There are a total of 3378 compounds and 12361 Fe-O bonds. The shortest bond length is 1.651 Å and the longest bond length is 2.629 Å.

Atom	Atom	Length/Å	Atom	Atom	Atom	Angle/ °	Atom	BVS (Fe ^{III})
Fe1	O1	1.824(8)	Fe1	O1	Fe2	129.4(4)	Fe1	2.91
Fe1	O2	1.986(10)	Fe1	O2	Fe2	116.7(4)	Fe2	3.07
Fe1	O3	1.976(9)	Fe1	O3	Fe2	98.4(3)	Fe3	2.76
Fe1	O5	1.925(4)	Fe1	O5	Fe2	99.8(18)	Fe4	3.15
Fe1	N1	2.226(5)	Fe1	O5	Fe4	117.4(19)		
Fe2	Cl1	2.315(15)	Fe3	O4	Fe2	112.9(3)		
Fe2	O1	2.047(8)	Fe3	O5	Fe4	86.7(4)		
Fe2	O2	1.996(9)	Fe4	O5	Fe2	140.8(2)		
Fe2	O3	2.015(8)						
Fe2	O4	1.978(7)						
Fe2	O5	2.025(4)						
Fe3	O4	1.917(7)						
Fe3	O5	2.492(9)						
Fe3	N2	2.336(8)						
Fe4	O5	1.999(4)						

Table S2. Pertinent bond lengths (Å) and angles (°) for **1**. The last column provides the BVS data for the four independent Fe ions.

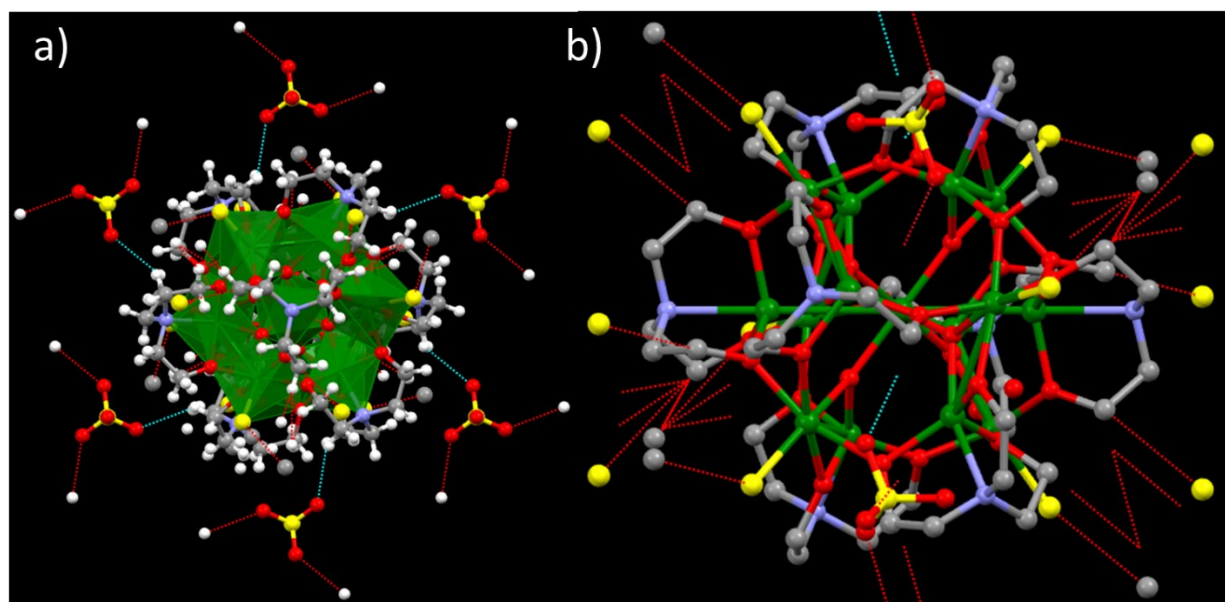


Figure S6. Closest intermolecular interactions between the perchlorate O-atoms and the C-atoms of the tea³⁻ ligands as viewed down the *c*-axis of the unit cell (a), and between the Cl ions and the C-atoms of the tea³⁻ ligands as viewed down the *b*-axis of the unit cell (b), at distances of ~3.4 Å. Colour code: Fe = green, O = red, N = blue, C = grey, Cl = yellow, H = white.

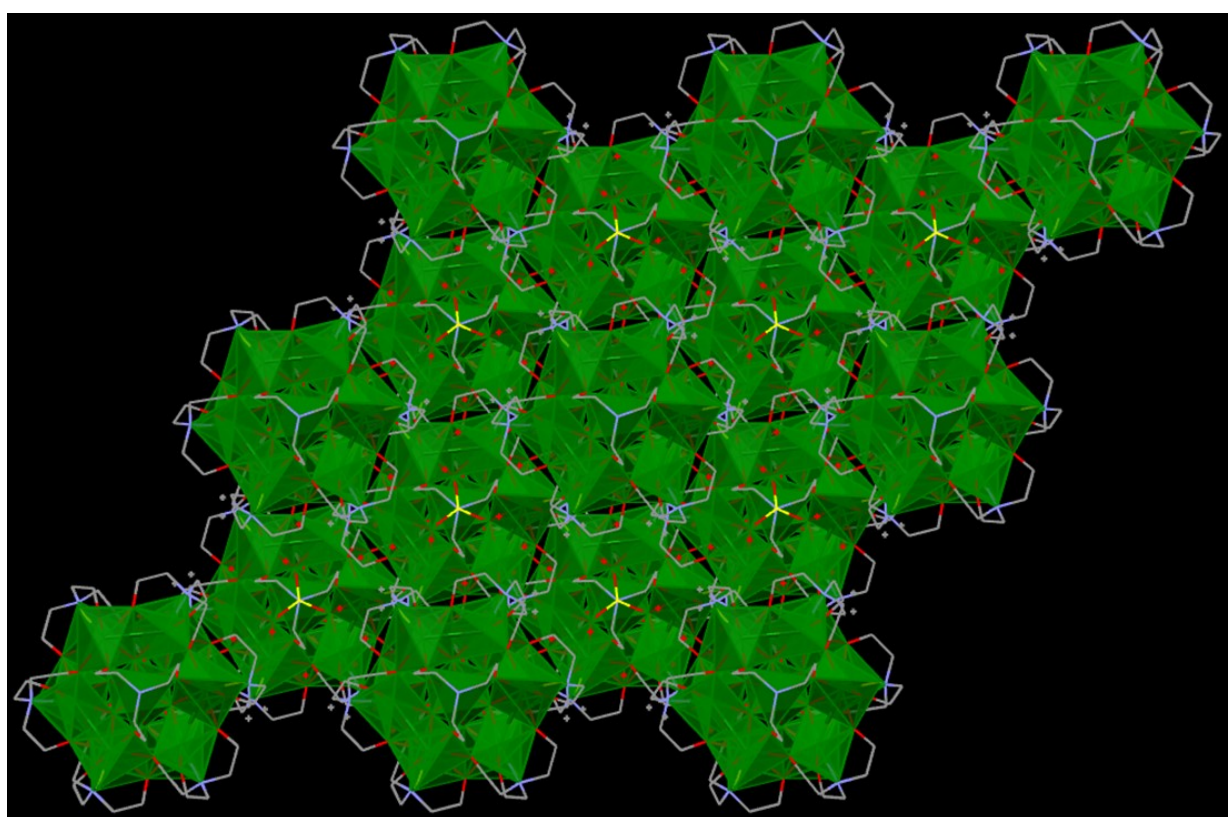


Figure S7. Packing of **1** in the extended structure, viewed down the *c*-axis of the unit cell. The Fe ions are given in polyhedral format. Colour code: Fe = green, O = red, N = blue, C = grey, Cl = yellow. H-atoms omitted.

Supporting Information

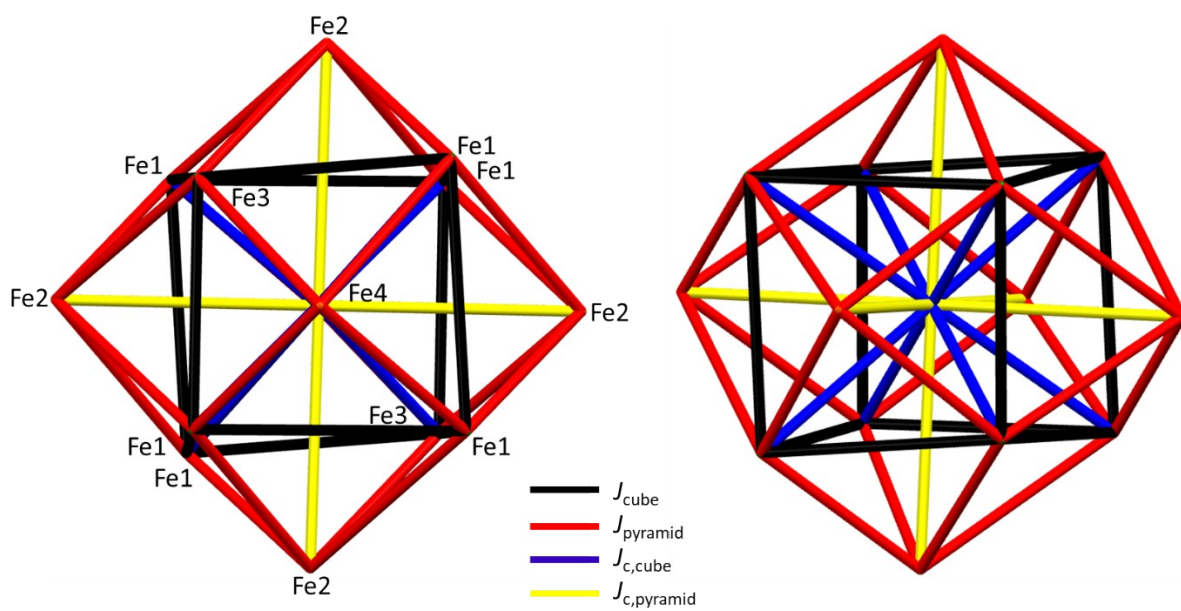


Figure S8. Exchange interaction scheme employed to simulate the magnetic susceptibility and magnetisation data of **1** using four J values (inset) and the finite temperature Lanczos method. The two figures show different orientations of the same scheme for clarity.

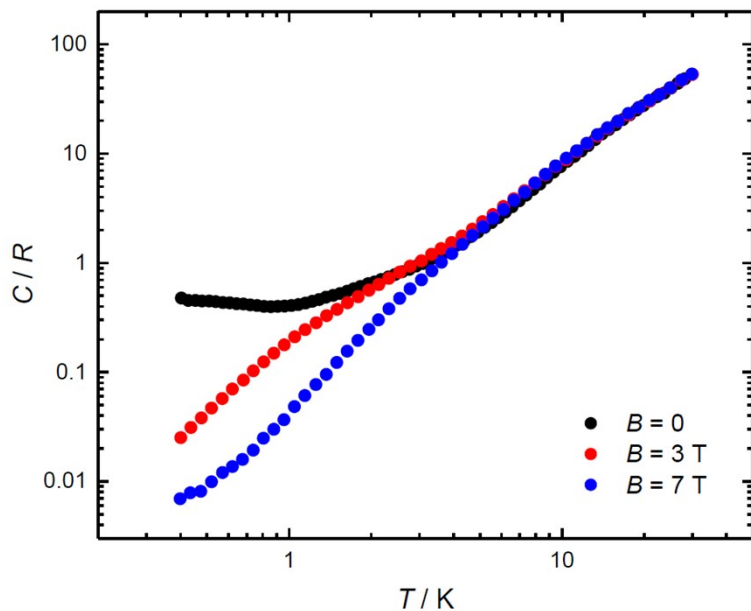


Figure S9. Heat capacity data for **1** in the indicated temperature and field ranges.

Computational details

Based on symmetry and structural parameters, there are a total of eight unique magnetic exchange interactions (J_1-J_8) present in **1**. These interactions are estimated using density functional theory (DFT) in the Gaussian 16 suite on model complex **1A** derived from **1** (Fig. S10).³ We have used the diamagnetic substitution method where we keep only the two paramagnetic Fe^{III} ions of interest and replace all others paramagnetic Fe^{III} metal ions with diamagnetic Ga^{III} ions. This method is known to be reliable for molecular systems with moderate magnetic exchange interactions.⁴⁻⁶ Noddleman's broken symmetry approach⁷ is used to calculate the magnetic exchange coupling constants. The B3LYP functional⁸⁻¹⁰ along with Ahlrichs TZV basis set¹¹⁻¹³ is used for Fe, Ga; and the 6-31G* basis set¹⁴ for Cl, O, N, C and H to estimate the magnetic exchange coupling constants. The methodology is known to reproduce the experimental J values for 3d metal clusters.^{5-6, 15-24}

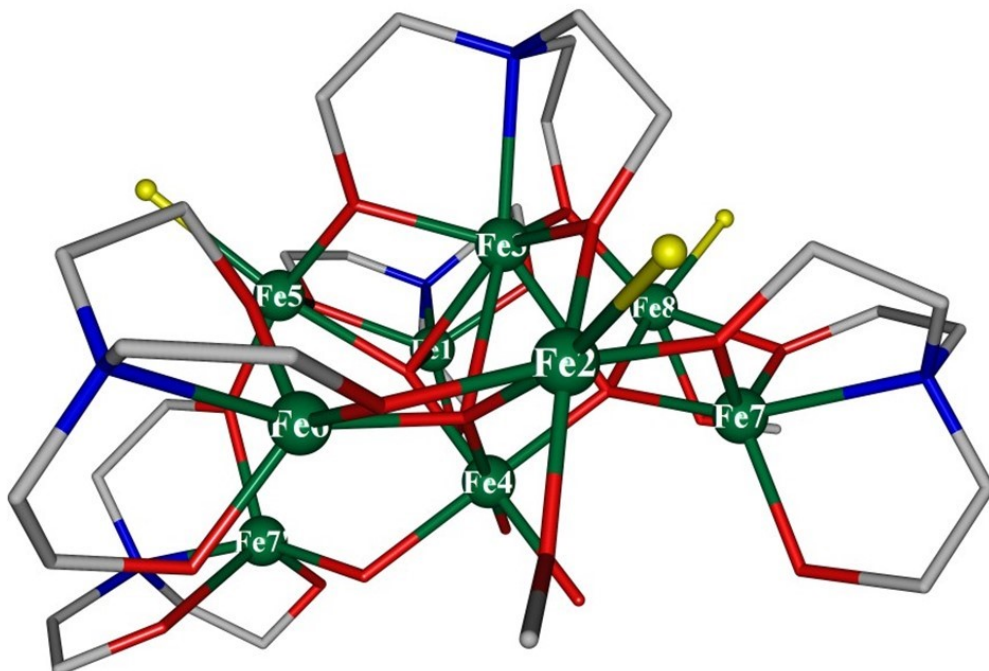
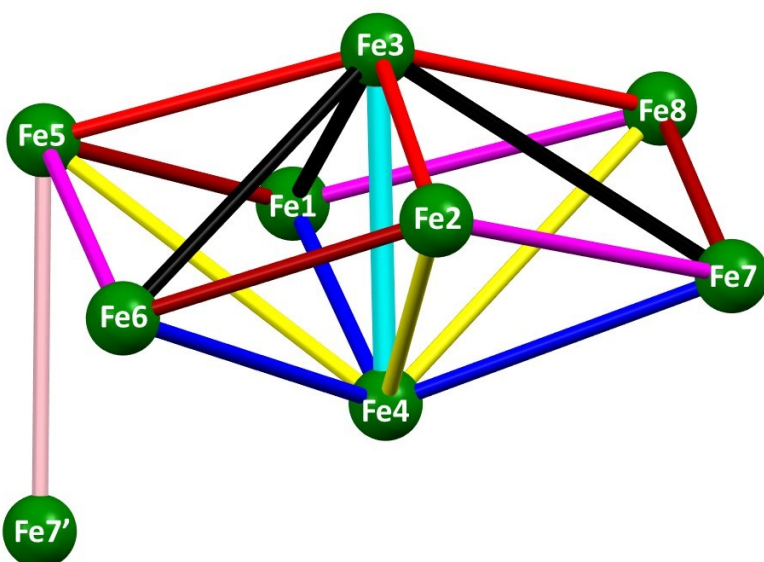


Figure S10. Model complex **1A** derived from **1**. Colour code as in Figure 2.



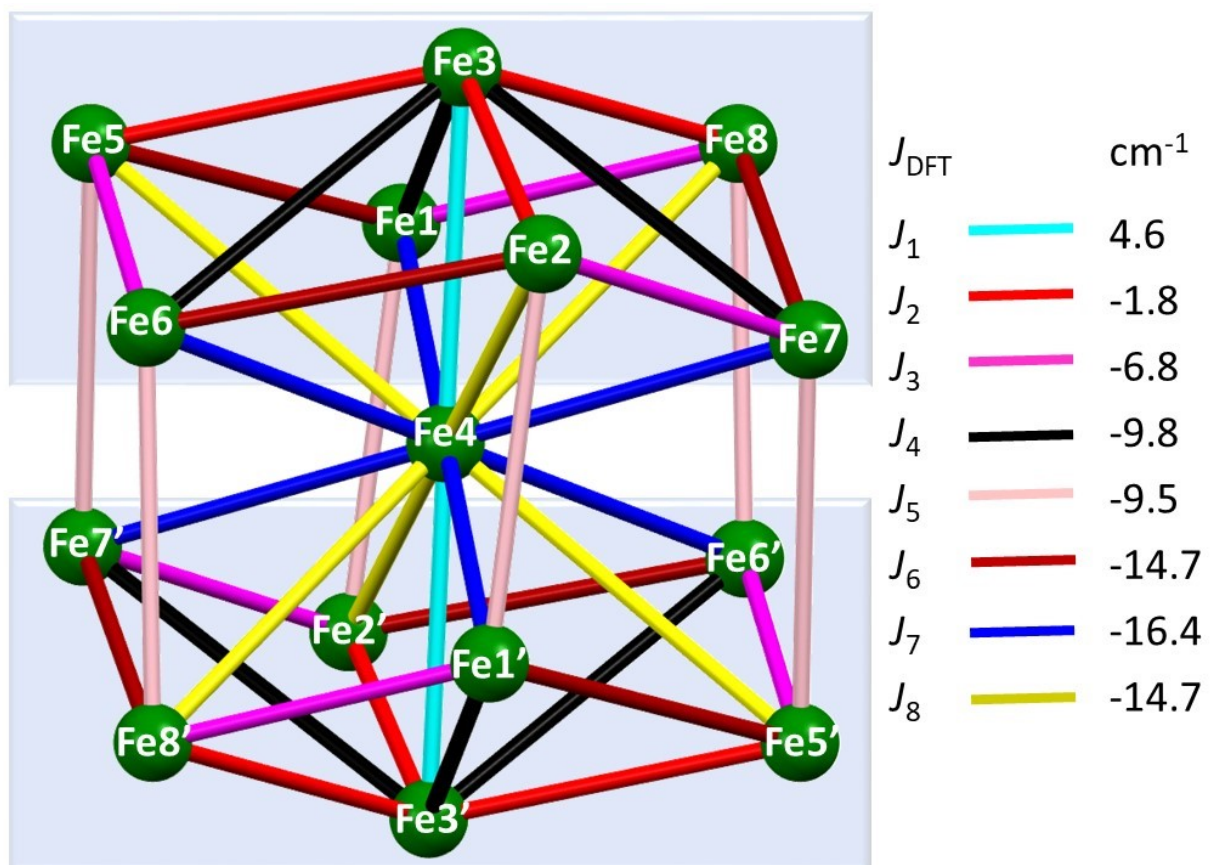


Figure S11. Schematic representation of the eight independent magnetic exchange interactions in model **1A** (top) and complex **1** (bottom).

Supporting Information

Table S3. DFT computed magnetic exchange interactions calculated for model complex **1A**, together with pertinent structural parameters for **1**. N = total number of individual interactions present. $\sum |S_{AB}|$ represents the total overlap integrals (OIs).

N J _{DFT}	Bridging group(s)	J / cm ⁻¹	Avg. Fe-O distance (Å)	Avg. Fe-O-Fe angle (°)	Fe-Fe distance (Å)	$\sum S_{AB}$
2 x J ₁	3 μ_4 -O ²⁻	+4.6	2.245	86.7	3.102	0.433
6 x J ₂	μ_2 -O-CH ₂ -CH ₂ -N(R), μ_4 -O ²⁻	-1.8	2.103	102.1	3.246	0.570
6 x J ₃	μ_2 -O-CH ₂ -CH ₂ -N(R), μ_4 -O ²⁻	-6.8	1.985	99.1	3.022	0.761
6 x J ₄	μ_4 -O ²⁻	-9.8	2.208	111.1	3.657	0.800
6 x J ₅	μ_2 -O-CH ₂ -CH ₂ -N(R)	-9.5	1.991	116.7	3.390	0.799
6 x J ₆	μ_2 -O-CH ₂ -CH ₂ -N(R)	-14.7	1.935	129.4	3.500	1.054
6 x J ₇	μ_4 -O ²⁻	-16.4	1.963	117.4	3.354	1.221
6 x J ₈	μ_4 -O ²⁻	-14.7	2.012	140.8	3.791	1.063

Table S4. DFT computed overlap integral (OI) values for J₁-J₈. Here α and β signify spin-up and spin-down orbitals, respectively. $\sum |S_{AB}|$ represents the total OIs between Fe^{III}-Fe^{III} SOMOs. Red and blue numbers represent strong and intermediate interactions, respectively. For the J₁ interaction, there is only one strong interaction (d_z^2 | d_{xz}), with the remaining 24 interactions all being weak. The overall result is a weak/moderate ferromagnetic interaction. For J₂ there are five intermediate interactions. J₃ and J₄ show one strong and three intermediate interactions, while J₅ has one strong and four intermediate interactions. The result is weak (J₂) or moderate (J₃-J₅) antiferromagnetic exchange interactions. For J₆-J₈, several strong and intermediate interactions result in strong antiferromagnetic exchange. The sign and magnitude of the DFT calculated magnetic exchange interactions are in excellent agreement with previously developed magneto-structural correlations¹⁶ which show that a larger average Fe^{III}-O-Fe^{III} angle and smaller average Fe^{III}-O distance increases the antiferromagnetic interaction (J₂-J₈), while smaller Fe^{III}-O-Fe^{III} angles and larger Fe^{III}-O distances increases the ferromagnetic interaction (J₁).

J ₁ = 4.6 cm ⁻¹ (α/β)	3d _{yz}	3d _{xz}	3d _z ²	3d _{xy}	3d _{x²-y²}	$\sum S_{AB} $
3d _{yz}	0.028	0.013	0.033	0.013	0.017	0.433
3d _{xy}	0.043	0.005	0.035	0.041	0.019	
3d _{xz}	0.000	0.001	0.104	0.012	0.004	
3d _z ²	0.004	0.012	0.001	0.002	0.008	
3d _{x²-y²}	0.011	0.006	0.006	0.004	0.011	
J ₂ = -1.8 cm ⁻¹ (α/β)	3d _{yz}	3d _{xz}	3d _z ²	3d _{xy}	3d _{x²-y²}	$\sum S_{AB} $
3d _{yz}	0.054	0.007	0.010	0.054	0.004	0.570
3d _{xy}	0.003	0.003	0.025	0.017	0.020	
3d _{xz}	0.068	0.005	0.009	0.009	0.009	
3d _{x²-y²}	0.005	0.001	0.006	0.029	0.010	
3d _z ²	0.046	0.039	0.018	0.060	0.059	
J ₃ = -6.8 cm ⁻¹ (α/β)	3d _{yz}	3d _{xy}	3d _{xz}	3d _{x²-y²}	3d _z ²	$\sum S_{AB} $
3d _{yz}	0.071	0.006	0.037	0.002	0.033	0.761
3d _{xy}	0.000	0.004	0.004	0.023	0.095	
3d _z ²	0.019	0.032	0.050	0.011	0.022	
3d _{xz}	0.029	0.003	0.044	0.162	0.014	
3d _{x²-y²}	0.012	0.041	0.005	0.024	0.018	

Supporting Information

$J_4 = -9.8 \text{ cm}^{-1} (\alpha/\beta)$	$3d_{yz}$	$3d_{xz}$	$3d_z^2$	$3d_{xy}$	$3d_{x^2-y^2}$	$\sum S_{AB} $
$3d_{yz}$	0.040	0.004	0.074	0.011	0.016	0.800
$3d_{xy}$	0.104	0.043	0.026	0.020	0.005	
$3d_{xz}$	0.091	0.029	0.033	0.003	0.005	
$3d_z^2$	0.092	0.041	0.027	0.024	0.012	
$3d_{x^2-y^2}$	0.018	0.003	0.016	0.027	0.036	
$J_5 = -9.5 \text{ cm}^{-1} (\alpha/\beta)$	$3d_{yz}$	$3d_{xy}$	$3d_{xz}$	$3d_{x^2-y^2}$	$3d_z^2$	$\sum S_{AB} $
$3d_{yz}$	0.033	0.006	0.027	0.004	0.078	0.799
$3d_{xy}$	0.010	0.010	0.014	0.027	0.020	
$3d_{xz}$	0.020	0.026	0.015	0.015	0.054	
$3d_z^2$	0.045	0.010	0.028	0.097	0.040	
$3d_{x^2-y^2}$	0.012	0.062	0.004	0.117	0.025	
$J_6 = -14.7 \text{ cm}^{-1} (\alpha/\beta)$	$3d_{yz}$	$3d_{xy}$	$3d_{xz}$	$3d_{x^2-y^2}$	$3d_z^2$	$\sum S_{AB} $
$3d_{yz}$	0.050	0.088	0.073	0.011	0.014	1.054
$3d_{xy}$	0.013	0.013	0.029	0.088	0.084	
$3d_{xz}$	0.001	0.034	0.009	0.000	0.041	
$3d_z^2$	0.010	0.012	0.006	0.109	0.007	
$3d_{x^2-y^2}$	0.011	0.047	0.002	0.226	0.076	
$J_7 = -16.4 \text{ cm}^{-1} (\alpha/\beta)$	$3d_{xy}$	$3d_{yz}$	$3d_{xz}$	$3d_z^2$	$3d_{x^2-y^2}$	$\sum S_{AB} $
$3d_{yz}$	0.029	0.105	0.047	0.009	0.103	1.221
$3d_{xy}$	0.02	0.068	0.012	0.072	0.066	
$3d_{xz}$	0.006	0.009	0.018	0.025	0.005	
$3d_z^2$	0.005	0.038	0.037	0.129	0.092	
$3d_{x^2-y^2}$	0.095	0.052	0.025	0.139	0.015	
$J_8 = -14.7 \text{ cm}^{-1} (\alpha/\beta)$	$3d_{yz}$	$3d_{xy}$	$3d_{xz}$	$3d_z^2$	$3d_{x^2-y^2}$	$\sum S_{AB} $
$3d_{yz}$	0.007	0.011	0.013	0.006	0.001	1.063
$3d_{xy}$	0.010	0.204	0.166	0.097	0.020	
$3d_{xz}$	0.026	0.002	0.006	0.037	0.019	
$3d_{x^2-y^2}$	0.008	0.044	0.049	0.091	0.066	
$3d_z^2$	0.027	0.038	0.007	0.055	0.053	

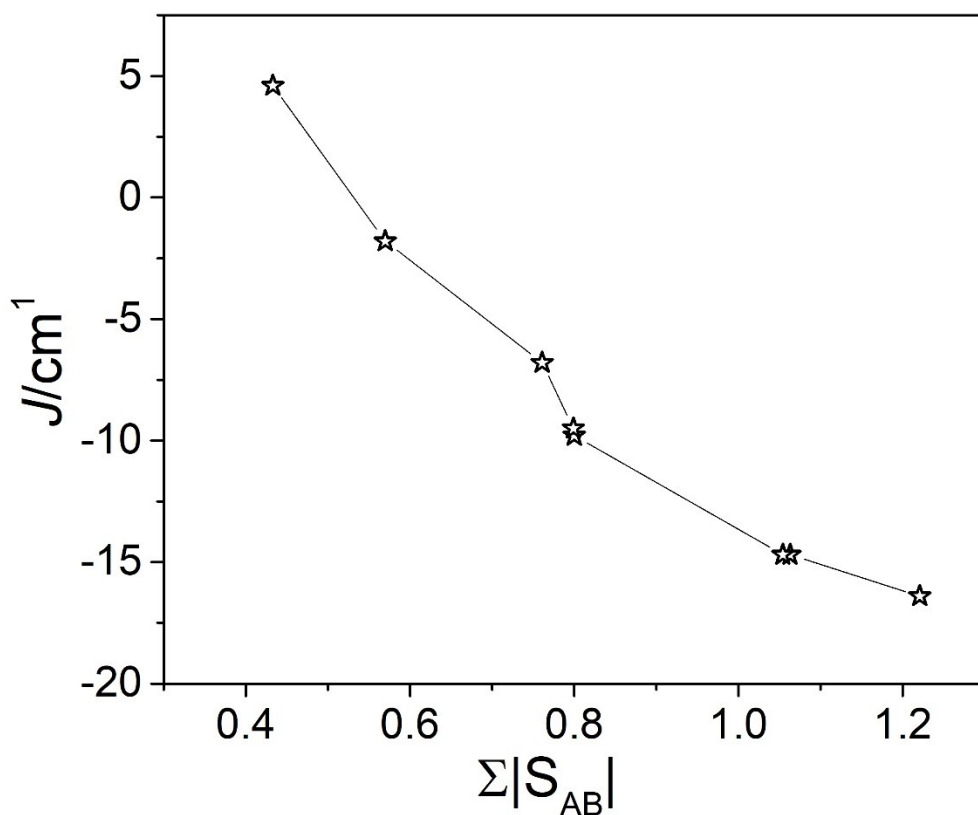
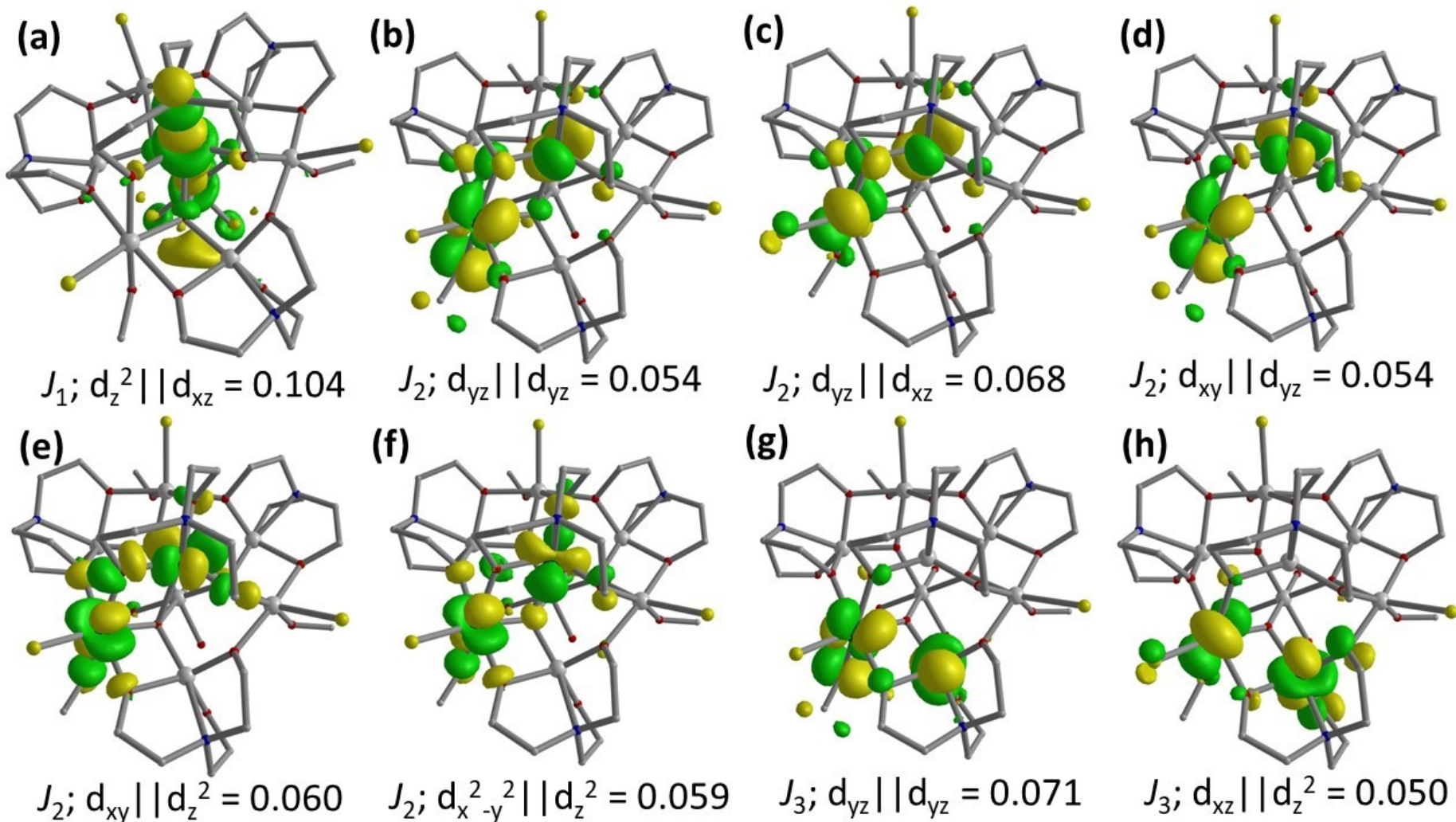
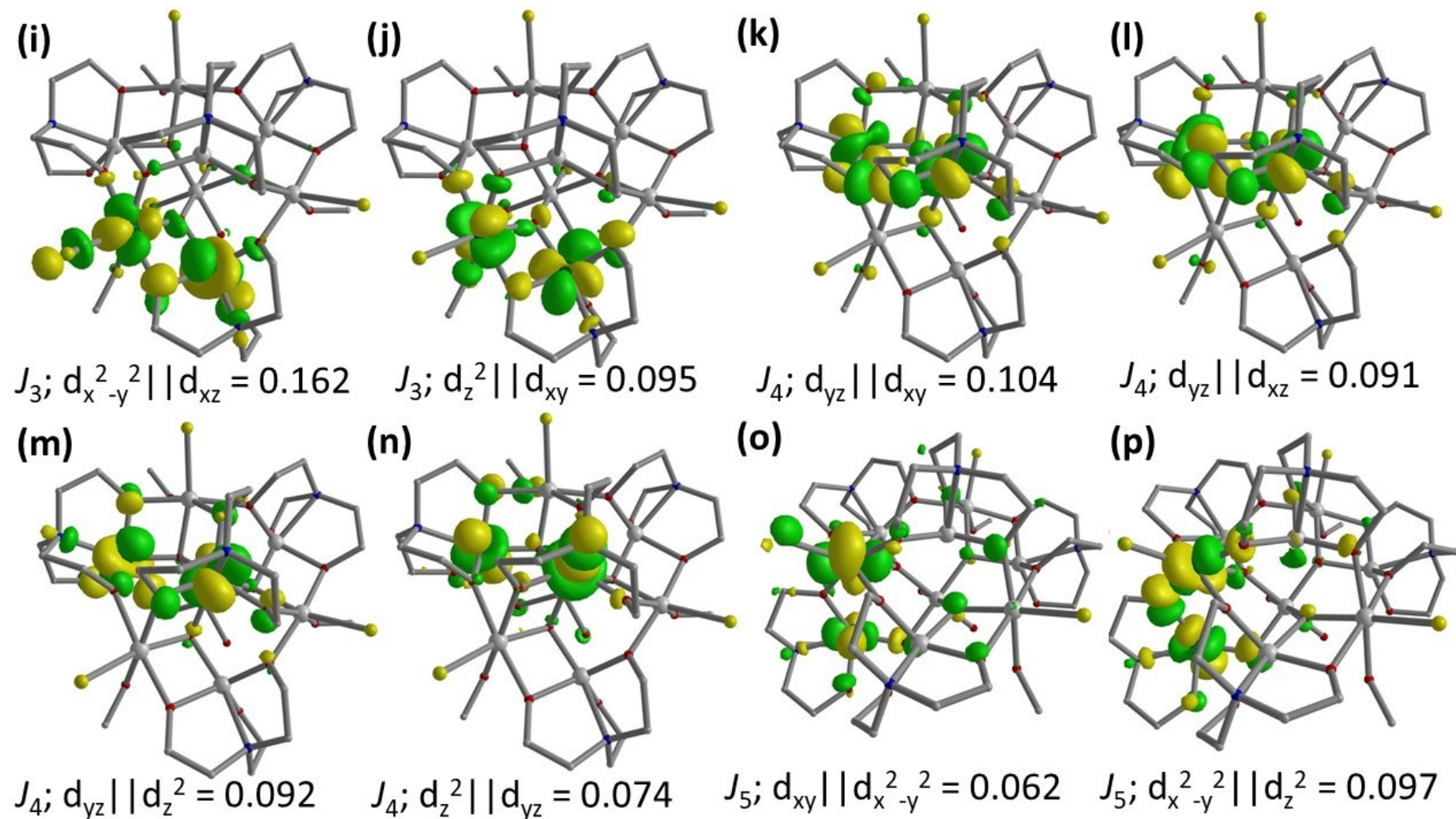
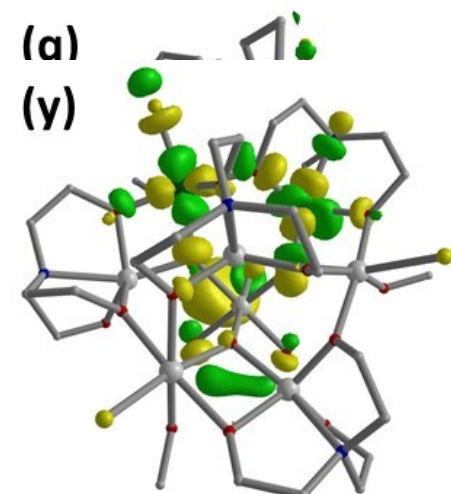


Figure S12. Plot of DFT estimated magnetic exchange interactions (J_1-J_8) with respect to their total overlap integral value ($\sum|S_{AB}|$). In general, larger the total overlap integral, the stronger the antiferromagnetic exchange interaction, and vice versa.⁶

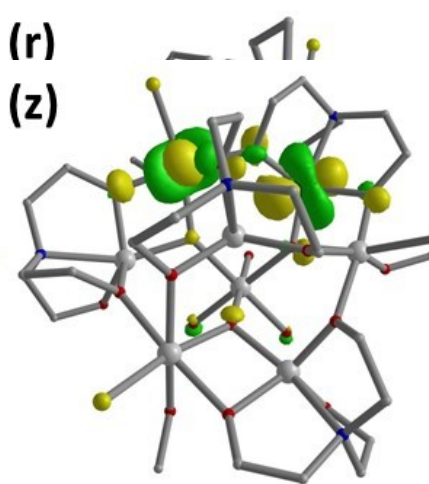


Supporting Information

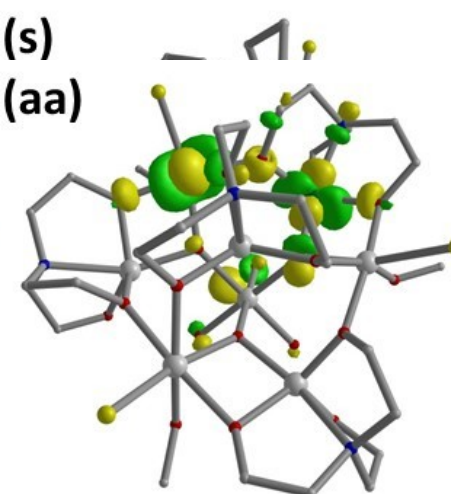




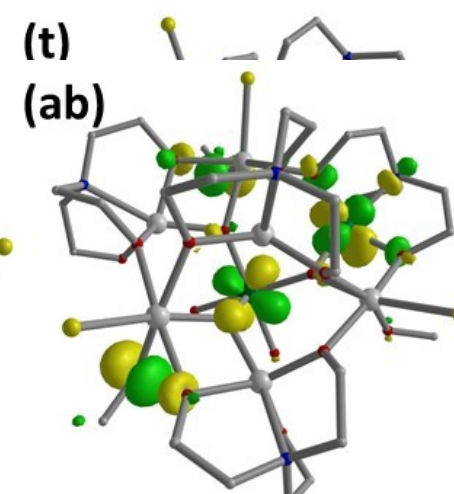
$$J_6; d_{x^2-y^2} || d_{x^2-y^2} = 0.226$$



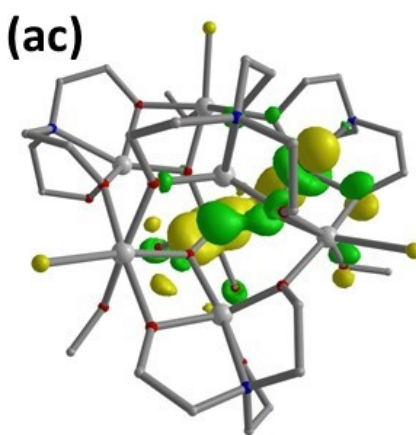
$$J_6; d_z^2 || d_{xy} = 0.084$$



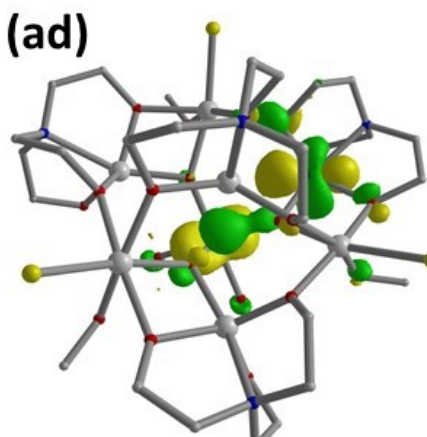
$$J_6; d_z^2 || d_{x^2-y^2} = 0.076$$



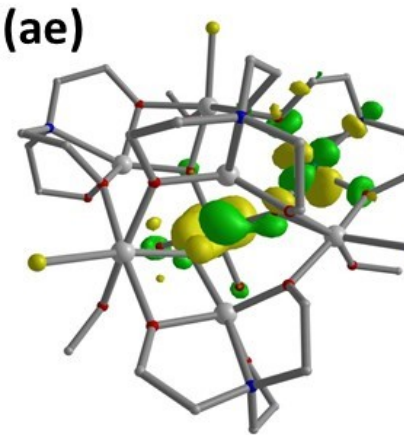
$$J_7; d_{xy} || d_{x^2-y^2} = 0.095$$



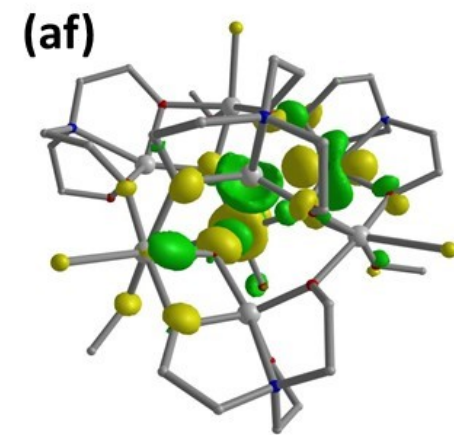
$$J_7; d_{yz} || d_{yz} = 0.105$$



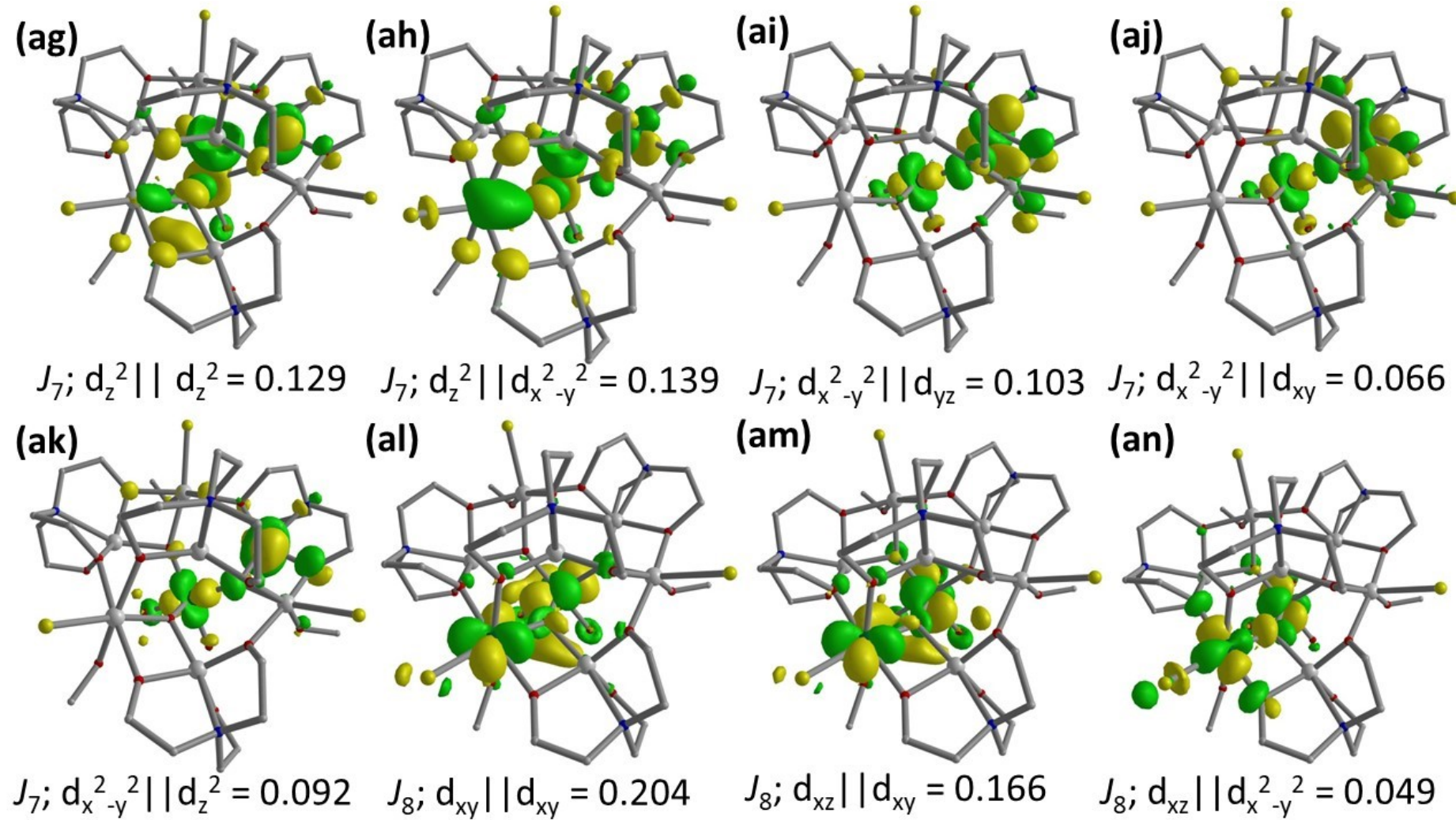
$$J_7; d_{yz} || d_{xy} = 0.068$$



$$J_7; d_{yz} || d_{x^2-y^2} = 0.052$$



$$J_7; d_z^2 || d_{xy} = 0.072$$



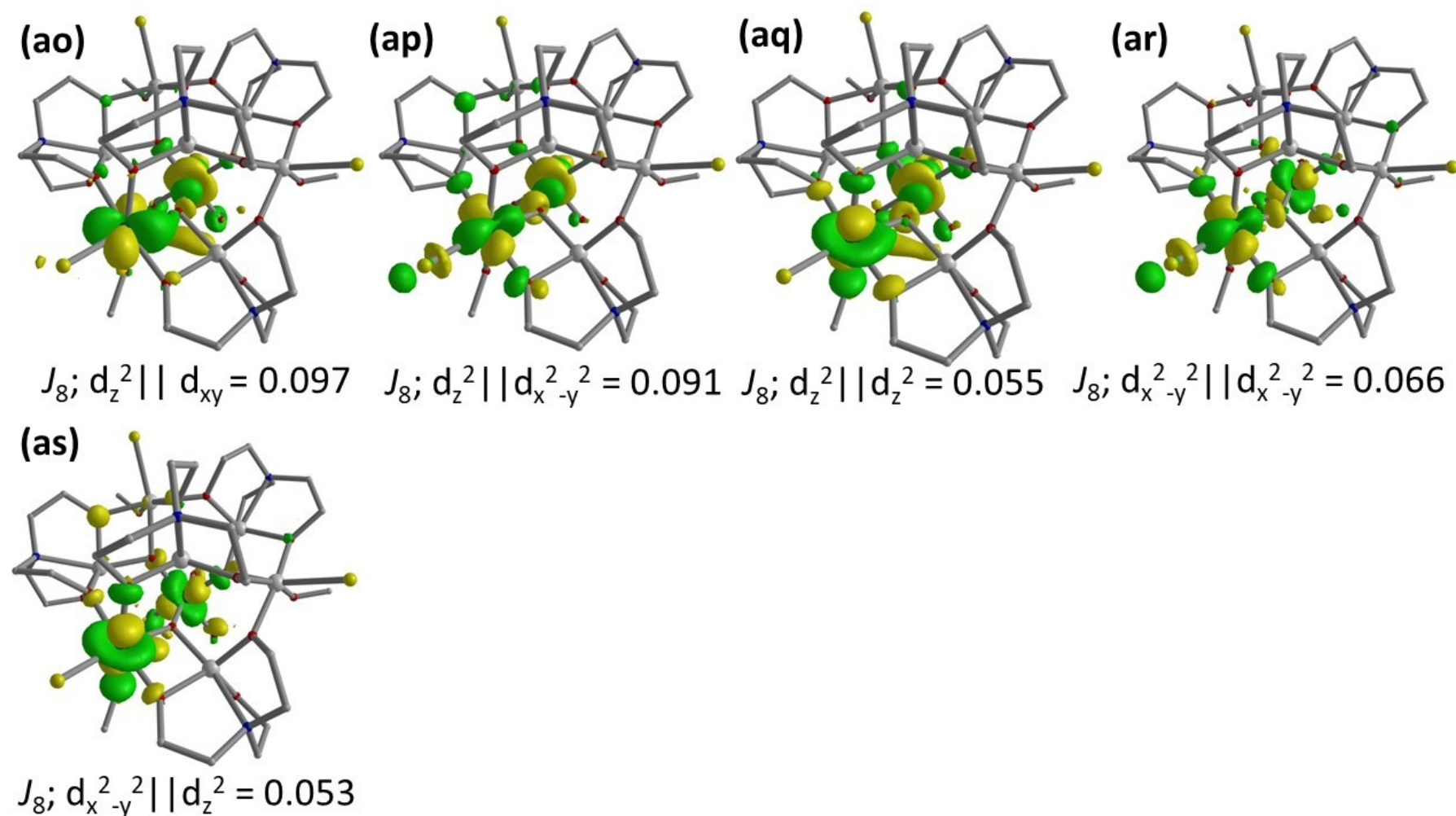


Figure S13. DFT calculated strong and intermediate overlap integrals corresponding to (a) J_1 ; (b-f) J_2 ; (g-j) J_3 ; (k-n) J_4 ; (o-s) J_5 ; (t-aa) J_6 ; (ab-ak) J_7 and (al-as) J_8 .

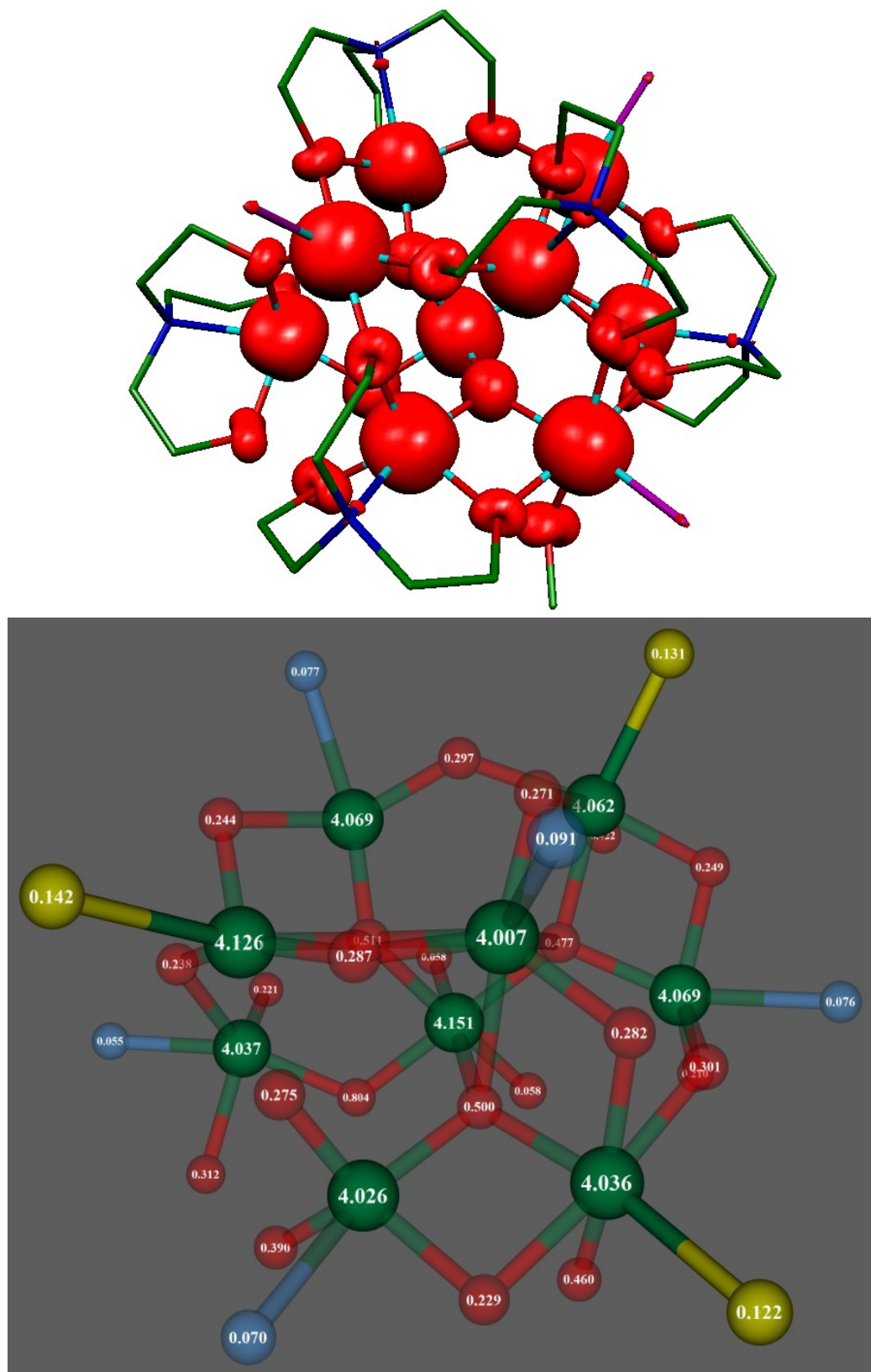


Figure S14. DFT computed spin density plot (top) together with the spin density values on the important atoms for model **1A** (bottom). Strong spin delocalization is observed for model **1A** with spin densities on the Fe^{III} ions ranging between 4.007-4.151.

References

1. G. M. Sheldrick, *Acta Crystallogr. Sect. C: Cryst. Struct. Commun.*, 2015, **71**, 3-8.
2. O. V. Dolomanov, L. J. Bourhis, R. J. Gildea, J. A. K. Howard and H. Puschmann, *J. Appl. Crystallogr.*, 2009, **42**, 339-341.
3. M. J. Frisch, G. W. Trucks, H. B. Schlegel, G. E. Scuseria, M. A. Robb, J. R. Cheeseman, G. Scalmani, V. Barone, G. A. Petersson, H. Nakatsuji, X. Li, M. Caricato, A. V. Marenich, J. Bloino, B. G. Janesko, R. Gomperts, B. Mennucci, H. P. Hratchian, J. V. Ortiz, A. F. Izmaylov, J. L. Sonnenberg, Williams, F. Ding, F. Lipparini, F. Egidi, J. Goings, B. Peng, A. Petrone, T. Henderson, D. Ranasinghe, V. G. Zakrzewski, J. Gao, N. Rega, G. Zheng, W. Liang, M. Hada, M. Ehara, K. Toyota, R. Fukuda, J. Hasegawa, M. Ishida, T. Nakajima, Y. Honda, O. Kitao, H. Nakai, T. Vreven, K. Throssell, J. A. Montgomery Jr., J. E. Peralta, F. Ogliaro, M. J. Bearpark, J. J. Heyd, E. N. Brothers, K. N. Kudin, V. N. Staroverov, T. A. Keith, R. Kobayashi, J. Normand, K. Raghavachari, A. P. Rendell, J. C. Burant, S. S. Iyengar, J. Tomasi, M. Cossi, J. M. Millam, M. Klene, C. Adamo, R. Cammi, J. W. Ochterski, R. L. Martin, K. Morokuma, O. Farkas, J. B. Foresman and D. J. Fox, Gaussian, Inc., Wallingford CT, 2016.
4. M. Coletta, S. Sanz, D. J. Cutler, S. J. Teat, K. J. Gagnon, M. K. Singh, E. K. Brechin and S. J. Dalgarno, *Dalton Trans.*, 2020, **49**, 14790-14797.
5. A. E. Dearle, D. J. Cutler, H. W. L. Fraser, S. Sanz, E. Lee, S. Dey, I. F. Diaz-Ortega, G. S. Nichol, H. Nojiri, M. Evangelisti, G. Rajaraman, J. Schnack, L. Cronin and E. K. Brechin, *Angew. Chem. Int. Ed.*, 2019, **58**, 16903-16906.
6. M. Coletta, T. G. Tziotzi, M. Gray, G. S. Nichol, M. K. Singh, C. J. Milius and E. K. Brechin, *Chem. Commun.*, 2021, **57**, 4122-4125.
7. L. Noodleman, *J. Chem. Phys.*, 1981, **74**, 5737.
8. A. D. Becke, *Phys. Rev. A*, 1988, **38**, 3098-3101.
9. A. D. Becke, *J. Chem. Phys.*, 1993, **98**, 5648.
10. C. Lee, W. Yang and R. G. Parr, *Phys. Rev. B: Condens. Matter Mater. Phys.*, 1988, **37**, 785.
11. A. Schäfer, H. Horn and R. Ahlrichs, *J. Chem. Phys.*, 1992, **97**, 2571-2577.
12. A. Schäfer, C. Huber and R. Ahlrichs, *J. Chem. Phys.*, 1994, **100**, 5829.
13. G. E. Scuseria and H. F. Schäfer, *J. Chem. Phys.*, 1989, **90**, 3700.
14. V. A. Rassolov, J. A. Pople, M. A. Ratner and T. L. Windus, *J. Chem. Phys.*, 1998, **109**, 1223-1229.
15. M. K. Singh, *Dalton Trans.*, 2020, **49**, 4539-4548.
16. M. K. Singh and G. Rajaraman, *Inorg. Chem.*, 2019, **58**, 3175-3188.
17. M. K. Singh and G. Rajaraman, *Chem. Eur. J.*, 2015, **21**, 980-983.
18. J. Caballero-Jiménez, F. Habib, D. Ramírez-Rosales, R. Grande-Aztatzi, G. Merino, I. Korobkov, M. K. Singh, G. Rajaraman, Y. Reyes-Ortega and M. Murugesu, *Dalton Trans.*, 2015, **44**, 8649.
19. C. McDonald, S. Sanz, E. K. Brechin, M. K. Singh, G. Rajaraman, D. Gaynor and L. F. Jones, *RSC Adv.*, 2014, **4**, 38182.
20. G. Rajaraman, E. Ruiz, J. Cano and S. Alvarez, *Chem. Phys. Lett.*, 2005, **415**, 6.
21. T. Cauchy, E. Ruiz and S. Alvarez, *J. Am. Chem. Soc.*, 2006, **128**, 15722-15727.
22. T. Cauchy, E. Ruiz and S. Alvarez, *Phys. B*, 2006, **384**, 116.
23. E. Ruiz, J. Cano and S. Alvarez, *Chem. Eur. J.*, 2005, **11**, 4767.
24. R. Carrasco, J. Cano, T. Mallah, L. F. Jones, D. Collison and E. K. Brechin, *Inorg. Chem.*, 2004, **43**, 5410-5415.